Miocene Antarctic ice sheet area adapts significantly faster than volume to CO_2-induced climate change

Lennert B. Stap[1], Constantijn J. Berends[1], and Roderik S.W. van de Wal[1,2]

[1]Institute for Marine and Atmospheric research Utrecht, Utrecht University, 3584 CC Utrecht, the Netherlands
[2]Department of Physical Geography, Faculty of Geosciences, Utrecht University, Utrecht, the Netherlands

Correspondence: L.B. Stap (L.B.Stap@uu.nl)

Abstract. The strongly varying benthic $\delta^{18}O$ levels of the early and mid-Miocene (23 to 14 Myr ago) are primarily caused by a combination of changes in Antarctic ice sheet (AIS) volume and deep ocean temperatures. These factors are coupled since AIS changes affect deep ocean temperatures. It has recently been argued that this is due to changes in ice sheet area rather than volume, because area changes affect the surface albedo. This finding would be important when the transient AIS grows relatively faster in extent than in thickness, which we test here. We analyse simulations of Miocene AIS variability carried out using the three-dimensional ice-sheet model IMAU-ICE forced by warm (high CO_2, no ice) and cold (low CO_2, large East-AIS) climate snapshots. These simulations comprise equilibrium and idealised quasi-orbital transient runs with strongly varying CO_2 levels (280 to 840 ppm). Our simulations show limited direct effect of East-AIS changes on Miocene orbital timescale benthic $\delta^{18}O$ variability, because of the slow build-up of volume. However, we find that relative to the equilibrium ice sheet size, the AIS area adapts significantly faster and more strongly than volume to the applied forcing variability. Consequently, during certain intervals the ice sheet is receding at the margins, while ice is still building up in the interior. That means the AIS does not adapt to a changing equilibrium size at the same rate or with the same sign everywhere. Our results indicate that the Miocene Antarctic ice sheet affects deep ocean temperatures more than its volume suggests.

1 Introduction

Orbital scale variability of benthic $\delta^{18}O$ levels during the early and mid-Miocene (23 to 14 Myr ago) primarily reflects changes in Antarctic Ice Sheet (AIS) volume and deep ocean temperatures. The separate contributions of these factors to the benthic $\delta^{18}O$ signal is fiercely debated. On one side of the argument, geological studies argue for strong AIS areal dynamism (Pekar and DeConto, 2006; Shevenell et al., 2008), with ice periodically advancing and retreating e.g. over Wilkes Land (Sangiorgi et al., 2018) and the Ross Sea sector (Hauptvogel and Passchier, 2012; Levy et al., 2016; Pérez et al., 2021). Oppositely, studies based on ice-proximal sea-surface temperature records from dinoflagellate cyst assemblages (Bijl et al., 2018) and TEX_{86} data (Hartman et al., 2018) call for limited AIS volume variability. Ice sheet modelling as deployed here can be used to reconcile AIS variability with the forcing climate evolution.

Ultimately, AIS volume and deep ocean temperatures changes are determined by insolation, regulated by the prevailing climatic background, e.g., geography (Stärz et al., 2017; Colleoni et al., 2018; Paxman et al., 2020; Halberstadt et al., 2021), vegetation (Knorr et al., 2011), and greenhouse gas concentrations (Frigola et al., 2021; Burls et al., 2021; Gasson et al., 2016; Halberstadt et al., 2021). AIS volume and ocean temperatures are in fact also directly related, because the AIS size affects sea water temperatures, doing so in different ways at different ocean depths. Climate model studies have found a spatially heterogeneous, but overall warming of Southern Ocean sea surface temperatures due to increasing AIS volume during the Middle Miocene Climatic Transition (MMCT; ∼14 million years ago), through the local wind field (Knorr and Lohmann, 2014) or through a decreased upwelling longwave flux over the elevated ice sheet (Frigola et al., 2021). These models also show a negligible (Knorr and Lohmann, 2014) or cooling (Frigola et al., 2021) response of deep ocean temperatures to an increasing AIS size. The contrasting responses between these studies can be ascribed to a difference in the implementation of ice sheet size changes. The former study (Knorr and Lohmann, 2014) only included the effect of ice thickness differences, keeping the ice area constant, whereas the latter (Frigola et al., 2021) also studied different AIS areal extents. A recent study confirmed that indeed ice area, rather than ice volume, affects deep ocean temperatures, because ice area impacts on the all-important surface albedo (Bradshaw et al., 2021).

This has ramifications for the partitioning between the contributions of AIS volume and deep ocean temperatures changes to benthic $\delta^{18}O$ levels during the early and mid-Miocene. The ice area may adapt significantly faster to climatic changes than ice volume, in other words the AIS may grow relatively more quickly in extent than in thickness. The effect of ice sheet changes on deep ocean temperatures can then vary comparatively more strongly than the ice sheet volume suggests. Whether this holds from an ice-physical perspective needs to be tested, preferably through transient AIS simulations in which the timescale of ice sheet adjustment is implicitly captured.

Here, we analyse simulations of Miocene AIS variability (Stap et al., 2022) carried out using the three-dimensional ice-sheet model IMAU-ICE (De Boer et al., 2014; Berends et al., 2018) forced by warm (high CO_2, no ice) and cold (low CO_2, large East-AIS) climate snapshots generated by the general circulation model GENESIS (Burls et al., 2021). The AIS simulations comprise idealised quasi-orbital transient runs (40 to 400 kyr timescales) with strongly varying CO_2 levels (280 to 840 ppm). We analyse these in relation to equilibrium simulations, in which the CO_2 level is kept constant over time. Utilising a recently developed matrix interpolation method (Berends et al., 2018), the climate forcing is interpolated based on CO_2 levels as well as varying ice sheet configurations, capturing key ice-sheet-atmosphere feedbacks. Stap et al. (2022) investigated the effect of including these feedbacks in the interpolation of climate forcing and found that their net effect is to reduce simulated transient Miocene Antarctic ice-sheet variability. Here, we focus on the relation between AIS volume and area and its effect on transient AIS growth and decay on orbital timescales. Our simulations corroborate the thesis put forth by Bradshaw et al. (2021) that the pre-MMCT AIS area adapts significantly faster than volume to equilibrium ice sheet changes caused by CO_2-induced climate change.

2 Models and methods

For this research, we analyse simulations of the AIS that were priorly conducted using the three-dimensional ice-sheet model
IMAU-ICE v1.1.1-MIO (De Boer et al., 2014; Berends et al., 2018; Stap et al., 2021). The model set-up and simulations are
described in detail in Stap et al. (2022), here we include a brief summary. IMAU-ICE combines the shallow ice approximation
(SIA) and shallow shelf approximation (SSA) to simulate the Antarctic ice sheet and shelf dynamics, on a 40-km square grid.
The groundling line is not treated in any special manner. The ice-free Antarctic bedrock topography and bathymetry are taken
from geological reconstructions of the early Miocene (24 to 23 Myr ago) (Paxman et al., 2019; Hochmuth et al., 2020a).

The basal mass balance underneath the floating ice shelves is parameterised (Pollard and DeConto, 2009; De Boer et al.,
2013), in part based on a linear relation to CO_2-dependent ocean temperature change (Beckmann and Goosse, 2003; Martin
et al., 2011; De Boer et al., 2013), while calving is not included. Though the ocean forcing has limited impact on our results
(Stap et al., 2022), the treatment of the mass balance of floating ice and of the grounding line in our current modelling effort
are in need of improvement (see Sect. 4). These are focal points of ongoing model development (Berends et al., 2022, 2023).

The surface mass balance is calculated using a simple but effective insolation-temperature-melt model (Bintanja et al., 2002;
Fettweis et al., 2020; Stap et al., 2022) with monthly forcing precipitation and surface air temperature input from pre-run
Miocene climate simulations by the general circulation model GENESIS v3.0 (Thompson and Pollard, 1997; DeConto et al.,
2012; Gasson et al., 2016; Burls et al., 2021). Using the Miocene global paleotopography from Herold et al. (2008) in com-
bination with specific Antarctic topography obtained from ice-sheet simulations by DeConto and Pollard (2003), and constant
present-day insolation, GENESIS simulates global climate on a T31 spectral resolution grid. Dynamic sea ice and vegetation
models ($2° \times 2°$ resolution) are connected to the atmospheric model, as well as a slab-ocean component (50-m resolution).
Here the Antarctic ice sheet is prescribed in the climate model (DeConto and Pollard, 2003; Burls et al., 2021), in contrast to
Gasson et al. (2016) who used GENESIS fully coupled to an ice-sheet model. Multiple GENESIS simulations were carried
out (Burls et al., 2021), of which we use a cold simulation forced with a CO_2 level of 280 ppm and a large East-Antarctic ice
sheet, and a warm simulation with 840 ppm CO_2 and no ice (Stap et al., 2022). Both simulations use a present-day orbital
configuration. A matrix interpolation method (Berends et al., 2018; Stap et al., 2022) is deployed to interpolate between warm
and cold simulations in order to obtain the transient forcing precipitation and surface air temperature fields applied at any time.
The interpolation is based on a combination of the (external) CO_2 forcing, and the simulated ice sheet, so that essential long-
term ice-sheet-atmosphere interactions are taken into account. These interactions affect both accumulation and ablation. They
include the albedo-temperature feedback, the surface-height-mass-balance feedback, and the ice-sheet desertification effect,
i.e., depletion of precipitation over ice sheets crescending in size (e.g. Oerlemans, 2004).

In this study, we investigate a simulation set consisting of eleven equilibrium and three transient simulations (Stap et al.,
2021) (Table 1) conducted using the model set-up described above. A detailed analyses of the equilibrium simulations was

previously performed (Stap et al., 2022, their reference experiment). Here they are used as a reference, as our focus is on transient ice area and ice volume variability in this study. The equilibrium simulations were conducted keeping the CO_2 concentration stable at various levels for 150 thousand model years, starting either with no ice (ascending branch) or with a developed ice sheet (return branch). In addition to the existing simulations, six extra equilibrium simulations were conducted for the current study at critical CO_2 levels where large ice volume changes take place: at 420, 448 and 476 ppm in the ascending branch, and at 644, 672 and 700 ppm in the return branch. In the transient simulations, the CO_2 level was lowered from 840 to 280 ppm in a linear fashion, and thereafter gradually raised back to 840 ppm. This V-pattern CO_2 forcing was executed in 100 kyr and 400 kyr. Finally, the CO_2 is sequentially varied five times in 200 kyr (40 kyr per cycle) (Fig. S1). We here analyse ice volume and ice area output generated every 1000 model years.

3 Results

In the transient simulations, the evolving ice sheet area and volume can be considered to be adjusting towards continuously changing equilibrium states (Stap et al., 2020). We distinguish three stages in the growth phase of the ice sheet (Fig. 1A-C, Table 2). Initially, the CO_2 level is lowered, and the ice sheet area and volume both grow, trailing behind the equilibrium ice sheet size (Fig. 2). Therefore, the difference between the (ascending branch) equilibrium volume and the transient volume, henceforth the volume deficit, increases. The volume growth rate increases approximately proportionally to this volume deficit during this stage (Fig. 3; pink and lightblue lines). In the subsequent second growth stage, after about 40% of the simulation time (40 kyr for the 100-kyr simulation, and 159 kyr for the 400-kyr simulation) the volume deficit starts to decrease. This is when the CO_2 level drops below 392 ppm and the increase of the equilibrium volume levels off. The transient ice area and volume are both still smaller than equilibrium and continue to increase (Fig. 2). Because the ice area is now larger than before, the ice volume accumulates over a wider area, causing the ice volume growth rates to be larger with respect to the ice volume deficit (Fig. 3; red and blue lines). After 52 kyr in the 100-kyr simulation and 201 kyr in the 400-kyr simulation, 52% and 50% of the total run time respectively, the transient ice area attains its maximum. We use a 10-kyr moving average to determine this turning point (Fig. S1B), because due to discretization flickering area variations occur when ice shelves are formed. In the ensuing third growth stage, the ice sheet area declines but because the ice thickness still increases in the interior, so does the total ice volume (Fig. 2). In contrast to growth stages I and II when volume growth was driven by area growth, the area now decreases and hence also the surface albedo. AIS variability consequently has a warming effect on deep ocean temperatures despite the growing volume (Bradshaw et al., 2021). During growth stage III, the ice volume growth rate quickly drops until the growth phase ends after 66 kyr (66% of the run) in the 100-kyr simulation and after 228 kyr (57% of the run) in the 400-kyr simulation (Fig. 3; brown and darkblue lines).

In both transient simulations, a similar maximum area is attained, meaning the ice sheet area is controlled more by the CO_2 level than by the ice-sheet-climate interaction. The effect of the AIS on deep ocean temperatures would therefore also be similar. The smaller volume-to-area ratio in the 100-kyr simulation compared to the 400-kyr simulation (Fig. S2) means that the

125   mean ice thickness and hence the surface height are lower. The ice sheet desertification effect is therefore reduced and hence precipitation rates are larger. As a result, the volume growth rates are much larger in the shorter 100-kyr simulation than in the 400-kyr simulation (Fig. 4A).

    Whereas the ice sheet growth rates vary rather smoothly, the waning phase of the ice sheet exhibits distinct periods of en-
130   hanced mass loss (Fig. 4B). Successive decay bursts in the 400-kyr simulation are related to ice sheet collapse in Coats Land, Princess Elizabeth Land, Wilkes Land and George V Land, Dome Fuji, Dome Circe and finally Dome Argus (Fig. S3). In the 100-kyr simulation, the collapse of Princess Elizabeth Land, Wilkes Land and George V Land, and of Dome Fuji and Dome Circe happen simultaneously (Figs. 1D and 5). Hence, peak decay rates are larger than in the 400-kyr simulation (Fig. 4B). Because ice sheet decay is more erratic than ice sheet growth, the relation between volume excess (the transient ice volume
135   minus the (return branch) equilibrium volume) and the volume decay rate (Fig. 6) is less straightforward than the relation between volume deficit and volume growth rates (Fig. 3). In general, our simulated Miocene AIS diminishes much faster than it grows, which causes a sawtooth shape of ice sheet variability similar to Pleistocene glacial cycles (Stap et al., 2019, 2022).

    In the 400-kyr simulation the CO_2 level is altered more gradually than in the 100-kyr simulation. The ice sheet remains
140   closer to equilibrium as it has more time to respond (Stap et al., 2022). It is furthermore clear that in our simulations the ice sheet area adapts relatively faster and more strongly to CO_2-induced climate change than the volume. In other words, the transiently varying ice sheet remains closer to the equilibrium extent than to the equilibrium volume. These differences in phase and relative amplitude (compared to the equilibrium size) between the responses of ice volume and area are also larger in the 100-kyr simulation than in the 400-kyr simulation, and they are magnified further still in our 40-kyr simulation (Figs. 2 and S1).

145 **4   Discussion**

AIS volume and deep ocean temperature changes constitute orbital timescale variations of benthic $\delta^{18}O$ levels during the early and mid-Miocene. These factors are determined by climate change, which in our simulations is induced by strongly varying CO_2 levels (280 to 840 ppm). Earlier ice-sheet modelling studies have shown that the relatively dry Antarctic climate, even during ice-free times, leads to a slow build-up of the AIS (Stap et al., 2019, 2022). This limits the variability of AIS on orbital
150   timescales, causing a reduced and delayed contribution to the benthic $\delta^{18}O$ signal (Fig. 7, green and purple lines). Through their direct effect on the climate and hence deep ocean temperatures, slow AIS changes would also imprint on the contribution of deep ocean temperatures to the benthic $\delta^{18}O$ signal. However, recent climate model studies have revealed that ice area, rather than ice volume, is decisive for this influence (Knorr and Lohmann, 2014; Frigola et al., 2021; Bradshaw et al., 2021), adding another factor to be considered. Here, we have shown that ice area adapts significantly faster to climate change than ice
155   volume. This is most clearly visible in our transient 40-kyr simulation as it covers multiple relatively short-term CO_2 cycles. In this simulation, the CO_2 level is varied between 280 and 840 ppm five consecutive times on a quasi-obliquity timescale (Table 1). The transient ice area maximum occurs earlier and has a larger magnitude than the ice volume volume, relative

to their maximum sizes as obtained from the 280-ppm equilibrium simulation (Fig. 7, cyan and purple lines). Consequently, the Antarctic ice sheet affects deep ocean temperatures generally more strongly than what can be inferred from ice volume variability. Arguably, this is partly due to the specifics of the matrix interpolation scheme for the climate forcing that we use. However, simulations using a simpler index method, in which the interpolation is solely based on the CO_2 level, show qualitatively similar results (Fig. S4). Our results provide the potential for a shorter lag between deep ocean temperature and climate (here CO_2) variability. In reality, this lag will depend first of all on how much deep ocean temperatures are affected by the AIS. Bradshaw et al. (2021) showed a simulated ~2 K decrease in deep ocean temperature caused by a drop in CO_2 from 850 to 280 ppm, and a further ~1 K added by the emergence of a continent-covering AIS. The climate-deep ocean lag will also depend on the timescale of deep ocean temperature adjustment, which we cannot constrain using our model set-up and needs to be investigated further. A shorter lag between deep ocean temperatures and climate would cause a further tipping of the balance towards a stronger contribution to Miocene benthic $\delta^{18}O$ variability by deep ocean temperatures compared to the contribution by ice volume changes.

In earlier research, the transiently evolving Miocene AIS was analysed in terms of adjustment towards changing equilibrium states (Stap et al., 2020). This analysis was performed using a model based on the notion that an ice sheet will grow when it is smaller and shrink when it is larger, than its explicitly prescribed equilibrium size. We have shown here, however, that it is not sufficient to regard the AIS as a whole in this respect. During our transient simulations, there are intervals when the margins of the ice sheet are receding while ice is still being built up in the interior. This discrepancy in phasing between area and volume affects the relation between the volume growth rate and volume deficit in the growth phase. In Sect. S1, we show that in our model a similar discrepancy in phasing between area and volume is exhibited by the North American ice sheet in settings representative for Pleistocene glacial-interglacial variability (Scherrenberg et al., 2023). This finding disputes conceptual models of glacial variability that (implicitly) assume identical timescales for ice area and ice volume adjustment.

The decay phase is characterised by periods of strongly enhanced ice mass loss. Thermodynamical instabilities are unlikely to be at the root of these decay bursts since basal temperatures remain below pressure melting point. Furthermore, the ice sheet is mostly grounded above sea level, and an additional simulation with LGM-like sub-shelf melt rates (Stap et al., 2022) shows similar peaks in ice melt (Fig. S6, green line), which also excludes instabilities due to ice-ocean interaction as the main cause of the bursts. A notable exception is the ice in the submarine Wilkes Basin, which decays significantly more gradually when sub-shelf melt is limited. We instead deduce feedbacks on the surface mass balance to be the instigator of the decay bursts. However, a simulation using a simpler index method, hence excluding the albedo-temperature feedback (Stap et al., 2022), also shows very similar periods of enhanced ice loss (Fig. S6, blue line). This points to the surface-height-mass-balance feedback as the primary cause: initial ice sheet decay triggers further climate warming through surface lowering, which causes further decay, etcetera.

Our model set-up will be extended in future research with some important factors that are still missing now. For instance, insolation changes, the ultimate driver of orbital variability, are not considered here. As a first step, they can be integrated in the matrix interpolation method (e.g. Ladant et al., 2014; Tan et al., 2018), but ultimately a carbon cycle model should be included in the model set-up to facilitate using insolation changes as the only external forcing (Ganopolski and Brovkin, 2017). Additionally, noisier forcing variability compared to our idealised smooth quasi-orbital forcing may reduce the mean size of the ice sheet (Niu et al., 2019; Stap et al., 2020). Furthermore, our simulations are aggravated by poorly represented ocean forcing (see Sect. 2). Ocean forcing was demonstrated to have limited impact on the transiently evolving AIS in the simulations investigated here, since AIS changes are mainly constricted to the East side of Antarctica (Stap et al., 2022). However, recent data (Marschalek et al., 2021) and modelling results (Gasson et al., 2016; Halberstadt et al., 2021) have made a case for a dynamic West AIS during the Miocene. Modelling the generally lower-lying West AIS requires an accurate incorporation of ocean forcing. This is currently being improved in IMAU-ICE (Berends et al., 2023), but outside the scope of our present effort. A related model improvement that will be deployed in future investigations of Miocene AIS variability concerns the grounding line physics (Berends et al., 2022). While this may increase the speed of ice sheet retreat, the main findings of our current study, which primarily concern the growth phase, will likely not be affected.

5   Conclusions

We have analysed equilibrium and idealised transient simulations of the response of the Miocene AIS to strong CO_2 variations (280 to 840 ppm). We relate the transient variability of ice area and volume to the changing equilibrium size pertaining to the prevailing CO_2 level. Our simulations support the premise that the relative growth of the transient Miocene AIS area significantly outpaces ice volume growth (Bradshaw et al., 2021). Consequently, also the relative magnitude of ice area variability is larger compared to ice volume. Ice area controls the effect of the AIS on deep ocean temperatures through surface albedo (Bradshaw et al., 2021). We therefore conclude that on orbital timescales during the early and mid-Miocene (pre-MMCT) the AIS affects deep ocean temperatures more than its volume suggests.

The discrepancy between ice area and ice volume growth means that the transiently changing ice sheet does not adjust towards equilibrium at the same rate or even with the same sign everywhere. Three stages can be distinguished during ice sheet growth. Initially, the ice area and mean thickness increase, trailing behind the growth of the equilibrium size. During the second stage, the equilibrium size levels off, but the transient ice area and thickness continue to increase. During the third stage, the ice sheet is receding at the margins, while ice is still building up in the interior. While during stages I and II the AIS has a cooling effect on deep ocean temperatures, this turns into a warming effect during stage III as the ice area declines. Finally, the decay phase of the AIS shows distinct periods of enhanced mass loss, which are most likely caused by the surface-height-mass-balance feedback.

Code availability. The code for IMAU-ICE v1.1.1-MIO is available from https://doi.org/10.5281/zenodo.6352125 (Berends and Stap, 2021).

Data availability. The model output analysed in this study is openly accessible from the PANGAEA database (Stap et al., 2021). The additional model output generated specifically for this study is accessible from Zenodo (Stap et al., 2023).

Author contributions. LBS designed the research and performed the experiments, with technical assistance from CJB. LBS, CJB, and RSWvdW analysed the results. LBS drafted the paper, with input from all co-authors.

Competing interests. The authors declare that they have no conflict of interest.

Acknowledgements. We acknowledge Fuyuki Saito and an anonymous reviewer for providing useful suggestions, which helped to improve the quality of the paper. We thank Edward Gasson for providing the GENESIS climate input data for our simulations, and Meike Scherrenberg for providing the model set-up for the Pleistocene North American ice-sheet simulations discussed in the Supplement. We further thank Gregor Knorr for commenting on an earlier draft of the manuscript. L.B. Stap is funded by the Dutch Research Council (NWO), through VENI grant VI.Veni.202.031. C.J. Berends was supported by PROTECT. This project has received funding from the European Union's Horizon 2020 research and innovation programme under grant agreement No 869304, PROTECT contribution number 83. Simulations were performed on the Gemini computing cluster of the Faculty of Science, Utrecht University.

References

Beckmann, A. and Goosse, H.: A parameterization of ice shelf–ocean interaction for climate models, Ocean Modelling, 5, 157–170, https://doi.org/10.1016/S1463-5003(02)00019-7, 2003.

Berends, C. J. and Stap, L. B.: IMAU-ICE v1.1.1-MIO archive, Zenodo [code], https://doi.org/10.5281/zenodo.6352125, 2021.

240   Berends, C. J., de Boer, B., and Van de Wal, R. S. W.: Application of HadCM3@Bristolv1.0 simulations of paleoclimate as forc-
      ing for an ice-sheet model, ANICE2.1: set-up and benchmark experiments, Geoscientific Model Development, 11, 4657–4675,
      https://doi.org/10.5194/gmd-11-4657-2018, 2018.

Berends, C. J., Goelzer, H., Reerink, T. J., Stap, L. B., and van de Wal, R. S. W.: Benchmarking the vertically integrated ice-sheet model
      IMAU-ICE (version 2.0), Geoscientific Model Development, 15, 5667–5688, https://doi.org/10.5194/gmd-15-5667-2022, 2022.

245   Berends, C. J., Stap, L. B., and van de Wal, R. S. W.: Strong impact of sub-shelf melt parameterisation on ice-sheet retreat in idealised and
      realistic Antarctic topography, Journal of Glaciology, p. 1—15, https://doi.org/10.1017/jog.2023.33, 2023.

Bijl, P. K., Houben, A. J. P., Hartman, J. D., Pross, J., Salabarnada, A., Escutia, C., and Sangiorgi, F.: Paleoceanography and ice sheet
      variability offshore Wilkes Land, Antarctica–Part 2: Insights from Oligocene–Miocene dinoflagellate cyst assemblages, Climate of the
      Past, 14, 1015–1033, https://doi.org/10.5194/cp-14-1015-2018, 2018.

250   Bintanja, R., Van de Wal, R. S. W., and Oerlemans, J.: Global ice volume variations through the last glacial cycle simulated by a 3-D
      ice-dynamical model, Quaternary International, 95, 11–23, https://doi.org/10.1016/S1040-6182(02)00023-X, 2002.

Bradshaw, C. D., Langebroek, P. M., Lear, C. H., Lunt, D. J., Coxall, H. K., Sosdian, S. M., and de Boer, A. M.: Hydrological impact of Middle
      Miocene Antarctic ice-free areas coupled to deep ocean temperatures, Nature Geoscience, 14, 429–436, https://doi.org/10.1038/s41561-
      021-00745-wT, 2021.

255   Burls, N. J., Bradshaw, C. D., De Boer, A. M., Herold, N., Huber, M., Pound, M., Donnadieu, Y., Farnsworth, A., Frigola, A., Gasson, E., et al.:
      Simulating Miocene warmth: insights from an opportunistic multi-model ensemble (MioMIP1), Paleoceanography and Paleoclimatology,
      p. e2020PA004054, https://doi.org/10.1029/2020PA004054, 2021.

Colleoni, F., De Santis, L., Montoli, E., Olivo, E., Sorlien, C. C., Bart, P. J., Gasson, E. G. W., Bergamasco, A., Sauli, C., Wardell,
      N., et al.: Past continental shelf evolution increased Antarctic ice sheet sensitivity to climatic conditions, Scientific Reports, 8, 1–12,
260   https://doi.org/10.1038/s41598-018-29718-7, 2018.

De Boer, B., Van de Wal, R. S. W., Lourens, L. J., Bintanja, R., and Reerink, T. J.: A continuous simulation of global ice volume over the
      past 1 million years with 3-D ice-sheet models, Climate Dynamics, 41, 1365–1384, https://doi.org/10.1007/s00382-012-1562-2, 2013.

De Boer, B., Lourens, L. J., and Van De Wal, R. S. W.: Persistent 400,000-year variability of Antarctic ice volume and the carbon cycle is
      revealed throughout the Plio-Pleistocene, Nature Communications, 5, 1–8, https://doi.org/10.1038/ncomms3999, 2014.

265   DeConto, R. M. and Pollard, D.: Rapid Cenozoic glaciation of Antarctica induced by declining atmospheric CO_2, Nature, 421, 245–249,
      https://doi.org/10.1038/nature01290, 2003.

DeConto, R. M., Pollard, D., and Kowalewski, D.: Modeling Antarctic ice sheet and climate variations during Marine Isotope Stage 31,
      Global and Planetary Change, 88-89, 45–52, https://doi.org/10.1016/j.gloplacha.2012.03.003, 2012.

Fettweis, X., Hofer, S., Krebs-Kanzow, U., Amory, C., Aoki, T., Berends, C. J., Born, A., Box, J. E., Delhasse, A., Fujita, K., Gierz, P.,
270   Goelzer, H., Hanna, E., Hashimoto, A., Huybrechts, P., Kapsch, M.-L., King, M. D., Kittel, C., Lang, C., Langen, P. L., Lenaerts, J. T. M.,
      Liston, G. E., Lohmann, G., Mernild, S. H., Mikolajewicz, U., Modali, K., Mottram, R. H., Niwano, M., Noël, B., Ryan, J. C., Smith, A.,
      Streffing, J., Tedesco, M., van de Berg, W. J., van den Broeke, M., van de Wal, R. S. W., van Kampenhout, L., Wilton, D., Wouters, B.,

Ziemen, F., and Zolles, T.: GrSMBMIP: intercomparison of the modelled 1980–2012 surface mass balance over the Greenland Ice Sheet, The Cryosphere, 14, 3935–3958, https://doi.org/10.5194/tc-14-3935-2020, 2020.

275 Frigola, A., Prange, M., and Schulz, M.: A dynamic ocean driven by changes in CO_2 and Antarctic ice-sheet in the middle Miocene, Palaeogeography, Palaeoclimatology, Palaeoecology, 579, 110 591, https://doi.org/10.1016/j.palaeo.2021.110591, 2021.

Ganopolski, A. and Brovkin, V.: Simulation of climate, ice sheets and CO_2 evolution during the last four glacial cycles with an Earth system model of intermediate complexity, Climate of the Past, 13, 1695–1716, https://doi.org/10.5194/cp-13-1695-2017, 2017.

Gasson, E., DeConto, R. M., Pollard, D., and Levy, R. H.: Dynamic Antarctic ice sheet during the early to mid-Miocene, Proceedings of the

280 National Academy of Sciences, 113, 3459–3464, https://doi.org/10.1073/pnas.1516130113, 2016.

Halberstadt, A. R. W., Chorley, H., Levy, R. H., Naish, T., DeConto, R. M., Gasson, E., and Kowalewski, D. E.: CO_2 and tectonic controls on Antarctic climate and ice-sheet evolution in the mid-Miocene, Earth and Planetary Science Letters, 564, 116 908, https://doi.org/10.1016/j.epsl.2021.116908, 2021.

Hartman, J. D., Sangiorgi, F., Salabarnada, A., Peterse, F., Houben, A. J. P., Schouten, S., Brinkhuis, H., Escutia, C., and Bijl, P. K.: Pa-

285 leoceanography and ice sheet variability offshore Wilkes Land, Antarctica–Part 3: Insights from Oligocene–Miocene TEX_{86}-based sea surface temperature reconstructions, Climate of the Past, 14, 1275–1297, https://doi.org/10.5194/cp-14-1275-2018, 2018.

Hauptvogel, D. W. and Passchier, S.: Early–Middle Miocene (17–14 Ma) Antarctic ice dynamics reconstructed from the heavy mineral provenance in the AND-2A drill core, Ross Sea, Antarctica, Global and Planetary Change, 82, 38–50, https://doi.org/10.1016/j.gloplacha.2011.11.003, 2012.

290 Herold, N., Seton, M., Müller, R. D., You, Y., and Huber, M.: Middle Miocene tectonic boundary conditions for use in climate models, Geochemistry, Geophysics, Geosystems, 9, https://doi.org/10.1029/2008GC002046, 2008.

Hochmuth, K., Gohl, K., Leitchenkov, G., Sauermilch, I., Whittaker, J. M., Uenzelmann-Neben, G., Davy, B., and De Santis, L.: The evolving paleobathymetry of the circum-Antarctic Southern Ocean since 34 Ma: A key to understanding past cryosphere-ocean developments, Geochemistry, Geophysics, Geosystems, 21, e2020GC009 122, https://doi.org/10.1029/2020GC009122, 2020a.

295 Knorr, G. and Lohmann, G.: Climate warming during Antarctic ice sheet expansion at the Middle Miocene transition, Nature Geoscience, 7, 376–381, https://doi.org/10.1038/ngeo2119, 2014.

Knorr, G., Butzin, M., Micheels, A., and Lohmann, G.: A warm Miocene climate at low atmospheric CO_2 levels, Geophysical Research Letters, 38, https://doi.org/10.1029/2011GL048873, 2011.

Ladant, J.-B., Donnadieu, Y., Lefebvre, V., and Dumas, C.: The respective role of atmospheric carbon dioxide and orbital parameters on ice

300 sheet evolution at the Eocene-Oligocene transition, Paleoceanography, 29, 810–823, https://doi.org/10.1002/2013PA002593, 2014.

Levy, R., Harwood, D., Florindo, F., Sangiorgi, F., Tripati, R., Von Eynatten, H., Gasson, E., Kuhn, G., Tripati, A., DeConto, R., et al.: Antarctic ice sheet sensitivity to atmospheric CO_2 variations in the early to mid-Miocene, Proceedings of the National Academy of Sciences, 113, 3453–3458, https://doi.org/10.1073/pnas.1516030113, 2016.

Marschalek, J. W., Zurli, L., Talarico, F., van de Flierdt, T., Vermeesch, P., Carter, A., Beny, F., Bout-Roumazeilles, V., Sangiorgi,

305 F., Hemming, S. R., et al.: A large West Antarctic Ice Sheet explains early Neogene sea-level amplitude, Nature, 600, 450–455, https://doi.org/10.1038/s41586-021-04148-0, 2021.

Martin, M. A., Winkelmann, R., Haseloff, M., Albrecht, T., Bueler, E., Khroulev, C., and Levermann, A.: The Potsdam Parallel Ice Sheet Model (PISM-PIK) – Part 2: Dynamic equilibrium simulation of the Antarctic ice sheet, The Cryosphere, 5, 727–740, https://doi.org/10.5194/tc-5-727-2011, 2011.

310 Niu, L., Lohmann, G., and Gowan, E. J.: Climate noise influences ice sheet mean state, Geophysical Research Letters, 46, 9690–9699, 2019.

Oerlemans, J.: Antarctic ice volume and deep-sea temperature during the last 50 Myr: a model study, Annals of Glaciology, 39, 13–19, https://doi.org/10.3189/172756404781814708, 2004.

Paxman, G. J. G., Jamieson, S. S. R., Hochmuth, K., Gohl, K., Bentley, M. J., Leitchenkov, G., and Ferraccioli, F.: Reconstructions of Antarctic topography since the Eocene–Oligocene boundary, Palaeogeography, Palaeoclimatology, Palaeoecology, 535, 109 346, https://doi.org/10.1016/j.palaeo.2019.109346, 2019.

Paxman, G. J. G., Gasson, E. G. W., Jamieson, S. S. R., Bentley, M. J., and Ferraccioli, F.: Long-Term Increase in Antarctic Ice Sheet Vulnerability Driven by Bed Topography Evolution, Geophysical Research Letters, 47, e2020GL090 003, https://doi.org/10.1029/2020GL090003, 2020.

Pekar, S. F. and DeConto, R. M.: High-resolution ice-volume estimates for the early Miocene: Evidence for a dynamic ice sheet in Antarctica, Palaeogeography, Palaeoclimatology, Palaeoecology, 231, 101–109, https://doi.org/10.1016/j.palaeo.2005.07.027, 2006.

Pérez, L. F., De Santis, L., McKay, R. M., Larter, R. D., Ash, J., Bart, P. J., Böhm, G., Brancatelli, G., Browne, I., Colleoni, F., et al.: Early and middle Miocene ice sheet dynamics in the Ross Sea: Results from integrated core-log-seismic interpretation, GSA Bulletin, https://doi.org/10.1130/B35814.1, 2021.

Pollard, D. and DeConto, R. M.: Modelling West Antarctic ice sheet growth and collapse through the past five million years, Nature, 458, 329–332, https://doi.org/10.1038/nature07809, 2009.

Sangiorgi, F., Bijl, P. K., Passchier, S., Salzmann, U., Schouten, S., McKay, R., Cody, R. D., Pross, J., Van De Flierdt, T., Bohaty, S. M., et al.: Southern Ocean warming and Wilkes Land ice sheet retreat during the mid-Miocene, Nature Communications, 9, 1–11, https://doi.org/10.1038/s41467-017-02609-7, 2018.

Scherrenberg, M. D. W., Berends, C. J., Stap, L. B., and van de Wal, R. S. W.: Modelling feedbacks between the Northern Hemisphere ice sheets and climate during the last glacial cycle, Climate of the Past, 19, 399–418, https://doi.org/10.5194/cp-19-399-2023, 2023.

Shevenell, A. E., Kennett, J. P., and Lea, D. W.: Middle Miocene ice sheet dynamics, deep-sea temperatures, and carbon cycling: A Southern Ocean perspective, Geochemistry, Geophysics, Geosystems, 9, https://doi.org/10.1029/2007GC001736, 2008.

Stap, L. B., Sutter, J., Knorr, G., Stärz, M., and Lohmann, G.: Transient variability of the Miocene Antarctic ice sheet smaller than equilibrium differences, Geophysical Research Letters, 46, 4288–4298, https://doi.org/10.1029/2019GL082163, 2019.

Stap, L. B., Knorr, G., and Lohmann, G.: Anti-phased Miocene ice volume and CO_2 Changes by transient Antarctic ice sheet variability, Paleoceanography and Paleoclimatology, 35, e2020PA003 971, https://doi.org/10.1029/2020PA003971, 2020.

Stap, L. B., Berends, C. J., Scherrenberg, M. D. W., van de Wal, R. S. W., and Gasson, E. G. W.: [dataset] Idealised steady-state and transient simulations of Miocene Antarctic ice-sheet variability using 3D thermodynamical ice-sheet model IMAU-ICE, PANGAEA, https://doi.org/10.1594/PANGAEA.939114, 2021.

Stap, L. B., Berends, C. J., Scherrenberg, M. D. W., Van De Wal, R. S. W., and Gasson, E. G. W.: Net effect of ice-sheet–atmosphere interactions reduces simulated transient Miocene Antarctic ice-sheet variability, The Cryosphere, 16, 1315–1332, https://doi.org/10.5194/tc-16-1315-2022, 2022.

Stap, L. B., Berends, C. J., and van de Wal, R. S. W.: [dataset] Additional steady-state simulations of Miocene Antarctic ice-sheet variability using 3D thermodynamical ice-sheet model IMAU-ICE, Zenodo [dataset], https://doi.org/10.5281/zenodo.10390154, 2023.

Stärz, M., Jokat, W., Knorr, G., and Lohmann, G.: Threshold in North Atlantic-Arctic Ocean circulation controlled by the subsidence of the Greenland-Scotland Ridge, Nature Communications, 8, 1–13, https://doi.org/10.1038/ncomms15681, 2017.

Tan, N., Ladant, J.-B., Ramstein, G., Dumas, C., Bachem, P., and Jansen, E.: Dynamic Greenland ice sheet driven by pCO_2 variations across the Pliocene Pleistocene transition, Nature Communications, 9, 1–9, https://doi.org/10.1038/s41467-018-07206-w, 2018.

Thompson, S. L. and Pollard, D.: Greenland and Antarctic mass balances for present and doubled atmospheric CO_2
from the GENESIS version-2 global climate model, Journal of Climate, 10, 871–900, https://doi.org/10.1175/1520-
0442(1997)010<0871:GAAMBF>2.0.CO;2, 1997.

350

Table 1. Description of the simulations analysed in this study. A present-day orbital configuration is used in all simulations.

Type	Initial conditions	CO$_2$ levels	Runtime (model years)
Equilibrium (ascending branch)	Miocene topography, no ice	280, 392, 420, 448, 476, 504, 616, 728, and 840 ppm	150 kyr
Equilibrium (return branch)	280-ppm equilibrium run	392, 504, 616, 644, 672, 700, 728, and 840 ppm	150 kyr
Transient	840-ppm equilibrium run	linearly from 840 to 280 to 840 ppm	100, 400, and 200 (5x40) kyr

Table 2. Indication of the change in mean ice thickness, ice area, volume deficit (equilibrium volume minus transient volume), and a description of the various stages during transient ice sheet variability.

Phase, stage	Thickness	Area	Deficit	Description
Growth I	Increases	Increases	Increases	Initial growth trails equilibrium
Growth II	Increases	Increases	Declines	Equilibrium volume levels off
Growth III	Increases	Declines	Declines	Thickness increase outweighs declining area
Decay	Declines	Declines	Negative (volume excess)	Decay occurs in bursts
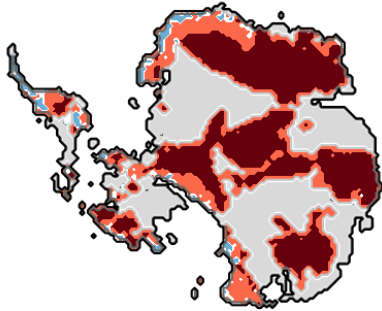
A) Stage I   **B) Stage II**
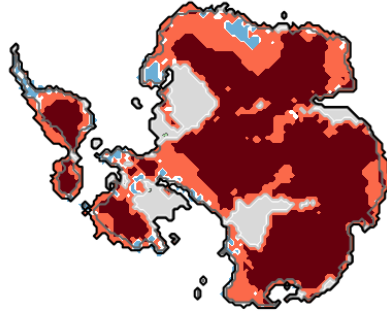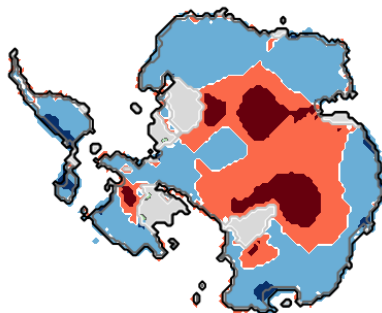
C) Stage III   **D) Decay**
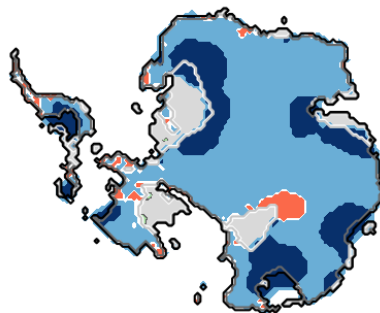
Figure 1. Change in Antarctic ice sheet thickness in the 100-kyr simulation, between **(A)** 30 kyr and 40 kyr (growth phase Stage I), **(B)** 40 kyr and 50 kyr (Stage II), **(C)** 60 kyr and 70 kyr (Stage III), and **(D)** 70 kyr and 80 kyr (decay phase). Red colors indicate ice thickness increase, blue colors decrease. Dark colors indicate where the ice thickness change exceeds 200 m over 10 kyr. No distinction is made here between ice shelf and grounded ice areas. Grey areas show where there is ice-free land and white areas show where there is ocean in both timesteps constituting the difference. Light grey lines indicate grounding lines or edges of the ice sheet on land, and dark lines coastlines obtained from the latest of the two timesteps that constitute the difference (40, 50, 70, and 80 kyr in all subpanels respectively).
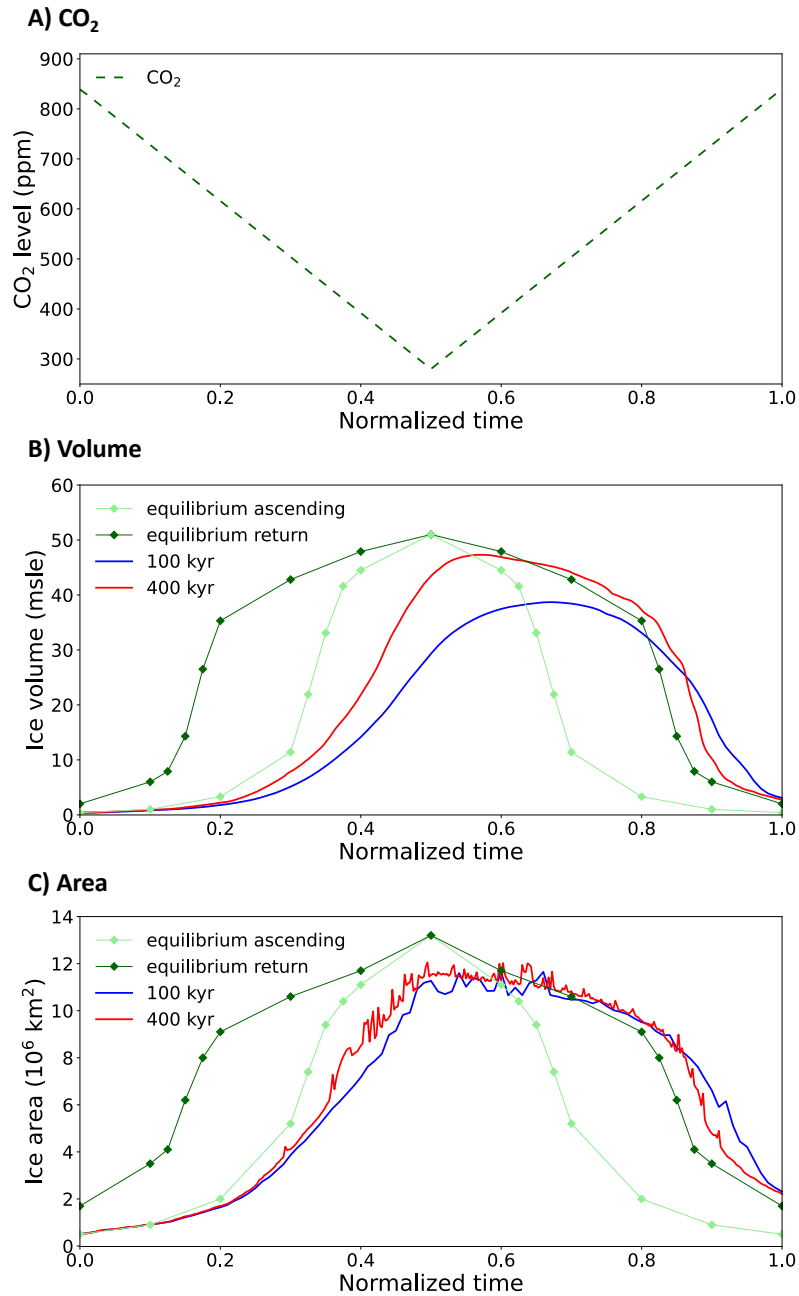
Figure 2. (**A**) Transient evolution of the forcing CO_2 level over time. (**B**) Same for the resulting ice volume, normalized with respect to the maximum integration time, for the 100-kyr (blue) and 400-kyr (red) simulations. (**C**) Same for the resulting ice area. The connected symbols indicate the ascending branch (lightgreen) and return branch (darkgreen) equilibrium ice volume and area pertaining to the prevailing CO_2 level.
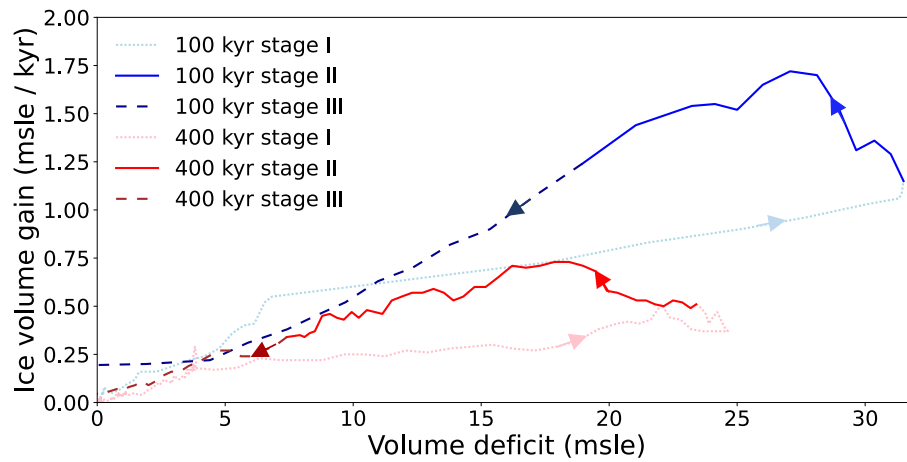
Figure 3. Growth rate plotted against the volume deficit, i.e., the difference between the (ascending branch) equilibrium volume and the transient volume, for the 100-kyr (blue) and 400-kyr (red) simulations. The different stages (I, II, and III) explained in the main text and Table 2, are indicated by varying color shades and dashes. The arrows indicate the progression direction.
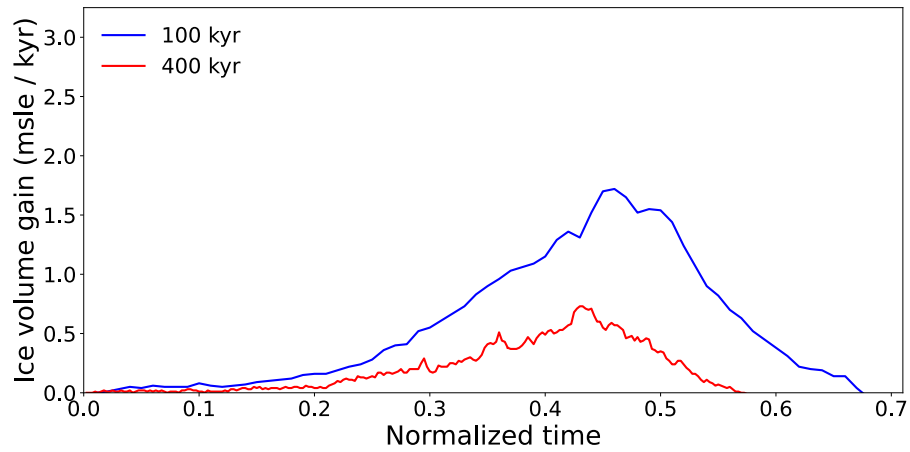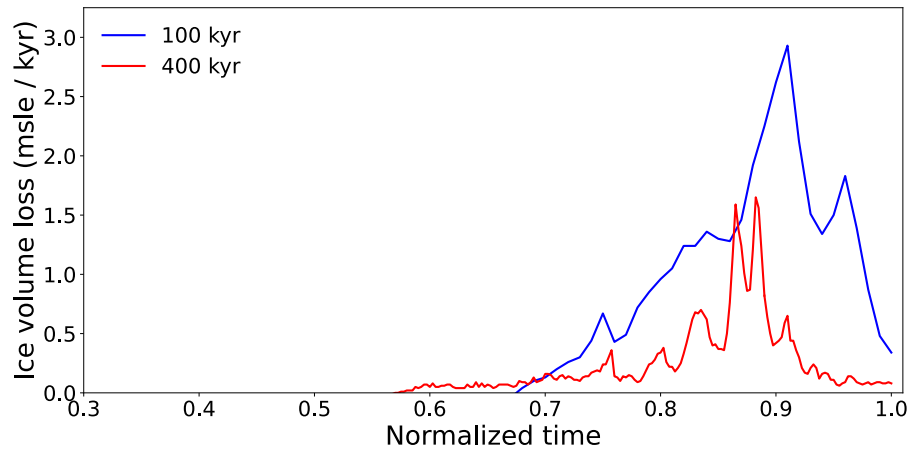
Figure 4. **(A)** Volume growth rate over normalized time, and **(B)** decay rate over time, for the 100-kyr (blue) and 400-kyr (red) simulations.
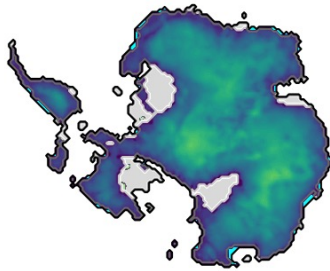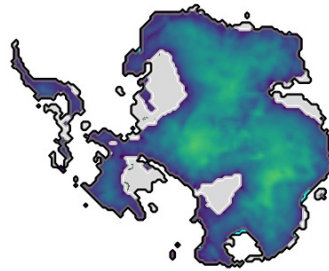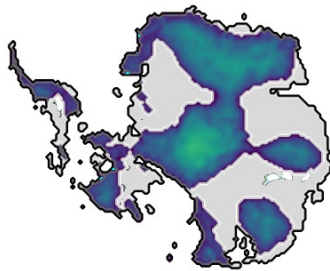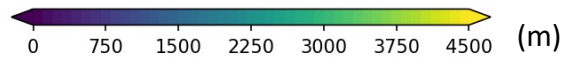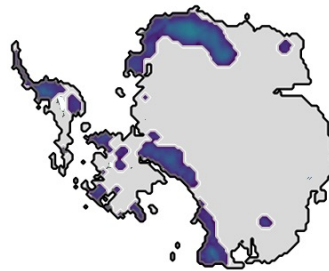
Figure 5. Maps of the ice thickness during the decay phase in the 100-kyr simulation, after **(A)** 70 kyr, **(B)** 80 kyr, **(C)** 90 kyr, and **(D)** 100 kyr. Grey areas indicate ice-free land and white areas ocean.
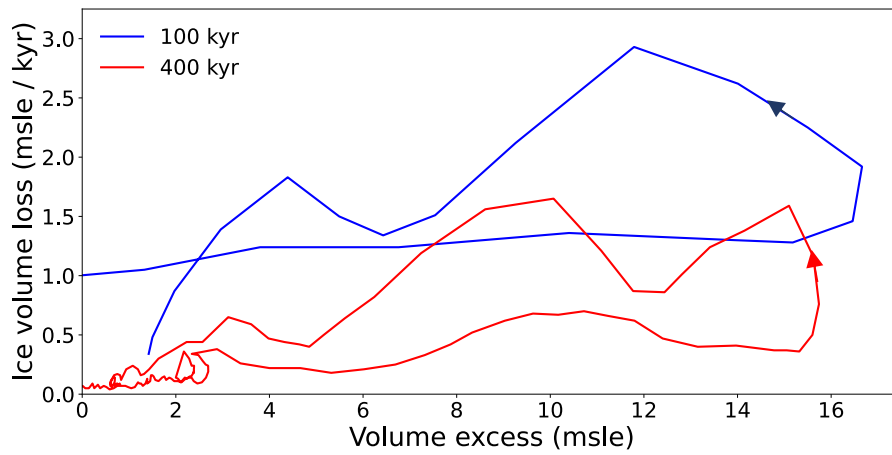
Figure 6. Volume decay rate plotted against the volume excess, i.e., the difference between the transient volume and the (return branch) equilibrium volume, for the 100-kyr (blue) and 400-kyr (red) simulations. The arrows indicate the progression direction.
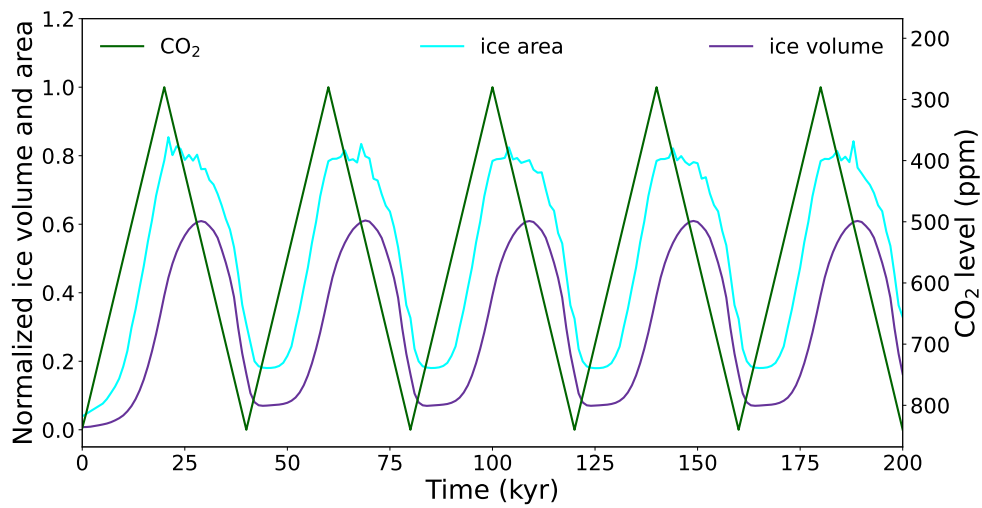
Figure 7. Transient evolution over time of ice area (cyan) and ice volume (purple) relative to their maximum sizes as obtained from the 280-ppm equilibrium simulation, 13.2×10^6 km^2 and 51.0 msle respectively, for the 40-kyr simulation. The green line shows the forcing CO_2 level. The right y-axis is reversed because CO_2 is generally negatively related to the benthic $\delta^{18}O$ signal.